



PROPERTIES OF INTERFACES AND PLASTIC DEFORMATION IN TiAl

V. PAIDAR

*Institute of Physics, Academy of Sciences
Na Slovance 2, 182 21 Praha 8, Czech Republic*

ABSTRACT

Complex plastic deformation of Ti-Al intermetallic alloys composed of lamellar microstructure is interpreted considering not only the forces acting on the carriers of plastic deformation but also the structure of these carriers in the crystal lattice. It is shown that a complicated nature of deformation processes when certain crystal defects under the same acting forces do sometimes contribute to the arising plastic strain but in other cases do not, can be explained by the asymmetry of twinning and of superdislocation motion. Moreover, both the special lamellar interfaces and general grain boundaries have a pronounced effect on plastic deformation, too.

KEYWORDS

Intermetallic compounds, modes of plastic deformation, superlattice dislocations, twinning, lamellar microstructure, grain boundaries, compatibility stresses.

INTRODUCTION

A large attention is currently paid to the Ti-rich Ti-Al ordered alloys that are considered as potential lightweight high-temperature structural materials for applications in the automotive and aerospace industries. The structure of tetragonal γ -phase of TiAl is of the $L1_0$ type. Since the parent lattice of $L1_0$ is only slightly different from the fcc lattice, cubic notation with the mixed parentheses $\{hkl\}$ and $\langle uvw \rangle$ is often utilised. These alloys contain also a minority hexagonal α_2 -phase of Ti_3Al with the $D0_{19}$ structure. Nevertheless, in this paper we will mostly concentrate on the interfaces in the $L1_0$ structure.

The microstructure of Ti-rich TiAl alloys is composed of lamellae of the γ - and α_2 -phases which are parallel to the closed packed atomic planes, i.e. to the octahedral (111) and basal (0001) planes in the nearly cubic and hexagonal lattices of $L1_0$ and $D0_{19}$, respectively. For the Ti-rich compositions close to the stoichiometric one, the α_2 -phase lamellae are narrow and not much frequent. Therefore, the majority of lamellar interfaces are of the γ - γ type. Each colony consisting of a single set of aligned lamellae represents a grain. Various types of the microstructure can be obtained by different processing. Special structures with elongated grains can be prepared using floating zone technique. The samples containing just one orientation of lamellae are called polysynthetically twinned (PST) crystals as they encompass a large number of twin interfaces [1,2]. The twist boundaries separating the neighbouring lamellae are special *rotational interfaces* on the $\{111\}$ planes for which the misorientation angle about the axis perpendicular to the interface plane is a multiple of 60° . In a bicrystal, the sample is composed only of two lamellar colonies. A tricrystal can be prepared from three

independent seeds etc. Generally, a polycrystal with texture composed of elongated grains can be grown by directional solidification. The boundaries separating the lamellar colonies can have arbitrary misorientation and also their plane, which is mostly parallel to the growth direction, is not fixed to any crystallographic direction. Those are in fact ordinary *grain boundaries* in a common sense of the usage of this term in the literature.

It was found by the quantitative study of the TiAl microstructure that the occurrence of two possible stacking sequences of the fcc lattice (ABC or CBA) in the $L1_0$ structure are equally probable [3]. This is apparently related to the fact that the sequences in the opposite directions induce the strain fields of the opposite sign during the formation of the γ -phase by the transformation from a high temperature hexagonal phase. In total, six different rotational variants of the γ -phase have to be distinguished in each grain. Three of them are associated with three different cubic axes, namely [100], [010] and [001], multiplied by two due to two different stackings of atomic planes parallel to the (111) interface, direct and reverse one.

The processes of plastic deformation associated with the interfaces in Ti-Al will be discussed in this paper. We will focus on the PST crystals loaded along the $\langle 101 \rangle$ and $\langle 121 \rangle$ growth axes, so called A1 and A2 orientations, respectively [4-6]. Besides the magnitude of the forces acting on dislocations due to the applied stress it is necessary to take into account asymmetrical nature not only of deformation twinning (the movement in the twinning or antitwining directions) but also of superdislocation glide. Usually, the dislocations can move along the glide plane equally in the forward or backward directions. However, because of the asymmetrical character of superdislocation cores, the motion of superdislocation in the $L1_0$ structure is possible only in certain direction while it cannot happen in the reverse sense. The rotational interfaces are efficient obstacles for dislocation motion as the processes of dislocation transmission take place there. Formation of dislocation pile-ups against the obstacles is further affected by additional compatibility stresses owing to anisotropic character of elastic and plastic strains.

This paper is divided into three sections. First, the activity of various deformation modes will be discussed on the basis of experimental observations of Kishida, Inui and Yamaguchi [5]. Next, the role of the lamellar interfaces played in the processes of plastic deformation will be assessed. And finally, the additional stresses that arise in the vicinity of the grain boundary between lamellar colonies due to compatibility requirements will be evaluated.

PLASTIC DEFORMATION OF PST CRYSTALS

Four types of deformation modes can carry plastic deformation in the $L1_0$ phase:

- a) slip of ordinary dislocations with the $1/2\langle 110 \rangle$ Burgers vectors,
- b) slip of the $\langle 101 \rangle$ superdislocations,
- c) slip of the $1/2\langle 112 \rangle$ superdislocations and
- d) twinning in the $\langle 112 \rangle$ direction.

All of these deformation modes operate on the $\{111\}$ close packed planes. $1/2\langle 110 \rangle$ are the lattice vectors contrary to $1/2\langle 101 \rangle$ which are the Burgers vectors of superpartials as the lattice vectors of $L1_0$, identical with the Burgers vectors of superdislocations, are $\langle 101 \rangle$. Similarly, the $1/2\langle 112 \rangle$ vectors are superlattice vectors, and hence they are the Burgers vectors of superdislocations, contrary to $1/2\langle 121 \rangle$ which are not the lattice vectors of $L1_0$. Three types of stacking faults can be involved in the structure of superlattice dislocations: antiphase boundaries (APB), superlattice intrinsic stacking faults (SISF) and complex

stacking faults (CSF) [7]. As both APB and CSF energies are high in TiAl, and moreover, APB can be even unstable [8], the dissociation of the $\langle 101 \rangle$ superdislocation is asymmetrical. The core of $\langle 101 \rangle$ is formed by a $1/6\langle 112 \rangle$ Shockley partial connected with the rest of dislocation by SISF (see Fig. 1a)

$$[\bar{1}01] = 1/6[\bar{5}\bar{1}4] + 1/6[\bar{1}\bar{1}2].$$

Similarly, the core of $1/2\langle 112 \rangle$ superdislocation is also asymmetrical

$$1/2[\bar{1}\bar{1}2] = 1/3[\bar{1}\bar{1}2] + 1/6[\bar{1}\bar{1}2].$$

These two dissociations are situated on one close packed plane of the $\{111\}$ type, and are hence both planar. Since the $\langle 101 \rangle$ direction lies in the intersection of two inclined $\{111\}$ planes, a wedge dissociation with the SISF segments on two different $\{111\}$ planes can occur (see Fig. 1b)

$$[\bar{1}01] = 1/3[\bar{2}01] + 1/6[\bar{1}\bar{1}2] + 1/6[\bar{1}\bar{1}\bar{2}]$$

and is thus sessile. The interaction forces between the partial dislocations that can enhance the transformation of glissile dislocation core into sessile configuration were studied by anisotropic elasticity in [9].

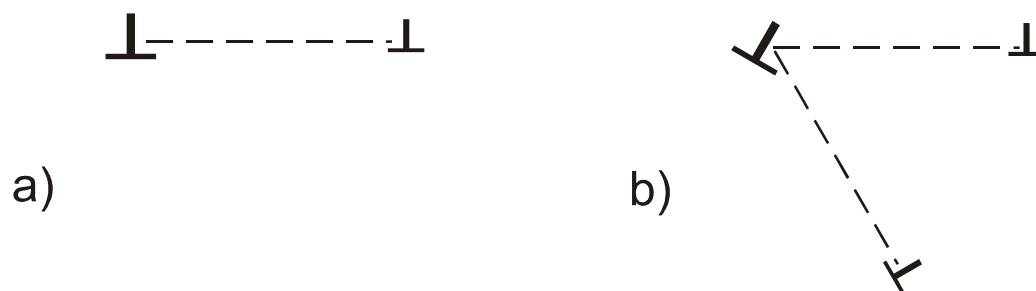


Fig. 1. Planar (glissile) and wedge (sessile) dissociations of the $\langle 101 \rangle$ superdislocation.

It is essential to define the sense of twinning directions. First we should know which crystal is displaced with respect to the other one. The shear deformation takes place on the $\{111\}$ planes. Let us start with the normals to these planes pointing upward, i.e. those having positive projections to the $[001]$ direction. If the loading axis lies near to $[001]$, the case of IIM and IIIM variants in A1 or IM variant in A2, all four $[11\bar{2}]$, $[1\bar{1}\bar{2}]$, $[\bar{1}1\bar{2}]$ and $[\bar{1}\bar{1}2]$ directions have twinning sense when the upper crystal is displaced with respect to the lower one. The shear deformation in these directions corresponds to compressive loading. The twinning directions are obviously reversed for tensile loading.

The primary factor controlling dislocation motion is the magnitude of the stress acting on the glide plane in the direction of the Burgers vector that is expressed by the Schmid factor. Except for the ordinary dislocations, the sense of the acting force is, however, equally important. When the deformation modes that are not permitted by the properties of dislocation cores are excluded, the number of possible modes listed in Tables 1, 2 and 4, 5 is substantially reduced. Tables 1, 2 are for tensile and compressive deformations of PST crystals with the A1 ($[\bar{1}10]$) orientation and Tables 4, 5 for the A2 ($[\bar{1}\bar{1}2]$) orientation. First, only true twinning in

the $\langle 112 \rangle$ direction can be considered as the pseudotwinning in $\langle 121 \rangle$ would require much higher energy. Similarly, the $\langle 121 \rangle$ superdislocations with the Burgers vectors twice as long as $1/2\langle 112 \rangle$ are unlikely to contribute to the plastic flow. The senses of twinning directions are summarized in Tables 3 and 6. The opposite antitwinning directions corresponding to the excluded deformation modes are grey-highlighted in Tables 1, 2 and 4, 5. On the contrary as it is observed, the $1/2\langle 112 \rangle$ superdislocations can move only in the antitwinning direction, and thus the slip directions in the twinning sense can be excluded as well. Finally, only the motion of $\langle 101 \rangle$ superdislocation in certain sense is permitted as discussed in more detail below. All the directions not allowed owing to the asymmetry of dislocation cores are grey-highlighted in Tables 1, 2 and 4, 5.

Table 1. Observed deformation modes in A1 ($[1\bar{1}10]$) PST crystal deformed in tension

The slip and twinning systems are arranged in such a way that the systems in each column have the same Schmid factors marked at the top of the table. The directions of ordinary dislocations and of true twinning with the largest Schmid factors are underlined. The observed systems [5] are in bold.

Schmid factors											
.000	<u>.408</u>	<u>-.408</u>	.000	<u>.408</u>	<u>-.408</u>	.000	.000	.000	.000	.000	.000
<u>.471</u>	-.236	-.236	<u>.471</u>	-.236	-.236	.000	.000	.000	.000	.000	.000
slip systems											
IM											
	-1 1 1			1 -1 1				-1 -1 1			1 1 1
1 1 0	<u>-1 0 -1</u>	<u>0 -1 1</u>	-1 -1 0	<u>1 0 -1</u>	<u>0 1 1</u>	-1 1 0	0 -1 -1	1 0 1	1 -1 0	0 1 -1	-1 0 1
<u>-1 1 -2</u>	-1 -2 1	2 1 1	<u>1 -1 -2</u>	1 2 1	-2 -1 1	-1 -1 -2	2 -1 1	-1 2 1	1 1 -2	-2 1 1	1 -2 1
IIM											
	1 1 -1			-1 1 1				-1 1 -1			1 1 1
1 0 1	<u>0 -1 -1</u>	<u>-1 1 0</u>	-1 0 -1	<u>0 -1 1</u>	<u>1 1 0</u>	1 0 -1	-1 -1 0	0 1 1	-1 0 1	1 -1 0	0 1 -1
1 -2 -1	-2 1 -1	<u>1 1 2</u>	-1 -2 1	2 1 1	<u>-1 1 -2</u>	-1 -2 -1	-1 1 2	2 1 -1	1 -2 1	1 1 -2	-2 1 1
IIIM											
	1 -1 1			1 1 -1				1 -1 -1			1 1 1
0 1 1	<u>-1 -1 0</u>	<u>1 0 -1</u>	0 -1 -1	<u>-1 1 0</u>	<u>1 0 1</u>	0 -1 1	-1 0 -1	1 1 0	0 1 -1	-1 0 1	1 -1 0
-2 -1 1	<u>1 -1 -2</u>	1 2 1	-2 1 -1	<u>1 1 2</u>	1 -2 -1	-2 -1 -1	1 2 -1	1 -1 2	-2 1 1	1 -2 1	1 1 -2
twinning systems											
IM											
	-1 1 1			1 -1 1				-1 -1 1			1 1 1
<u>-1 1 -2</u>	-1 -2 1	2 1 1	<u>1 -1 -2</u>	1 2 1	-2 -1 1	-1 -1 -2	2 -1 1	-1 2 1	1 1 -2	-2 1 1	1 -2 1
IIM											
	1 1 -1			-1 1 1				-1 1 -1			1 1 1
1 -2 -1	-2 1 -1	<u>1 1 2</u>	-1 -2 1	2 1 1	<u>-1 1 -2</u>	-1 -2 -1	-1 1 2	2 1 -1	1 -2 1	1 1 -2	-2 1 1
IIIM											
	1 -1 1			1 1 -1				1 -1 -1			1 1 1
-2 -1 1	<u>1 -1 -2</u>	1 2 1	-2 1 -1	<u>1 1 2</u>	1 -2 -1	-2 -1 -1	1 2 -1	1 -1 2	-2 1 1	1 -2 1	1 1 -2

Table 2. Observed deformation modes in A1 ($[\bar{1}10]$) PST crystal deformed in **compression**

Schmid factors											
.000	<u>-.408</u>	<u>.408</u>	.000	<u>-.408</u>	<u>.408</u>	.000	.000	.000	.000	.000	.000
<u>-.471</u>	.236	.236	<u>-.471</u>	.236	.236	.000	.000	.000	.000	.000	.000
slip systems											
IM											
	-1 1 1			1 -1 1			-1 -1 1			1 1 1	
1 1 0	-1 0 -1	0 -1 1	-1 -1 0	1 0 -1	0 1 1	-1 1 0	0 -1 -1	1 0 1	1 -1 0	0 1 -1	-1 0 1
<u>-1 1 -2</u>	-1 -2 1	2 1 1	<u>1 -1 -2</u>	1 2 1	-2 -1 1	-1 -1 -2	2 -1 1	-1 2 1	1 1 -2	-2 1 1	1 -2 1
IIM											
	1 1 -1			-1 1 1			-1 1 -1			1 1 1	
1 0 1	0 -1 -1	-1 1 0	-1 0 -1	0 -1 1	1 1 0	1 0 -1	-1 -1 0	0 1 1	-1 0 1	1 -1 0	0 1 -1
1 -2 -1	-2 1 -1	1 1 2	-1 -2 1	2 1 1	-1 1 -2	-1 -2 -1	-1 1 2	2 1 -1	1 -2 1	1 1 -2	-2 1 1
IIIM											
	1 -1 1			1 1 -1			1 -1 -1			1 1 1	
0 1 1	-1 -1 0	1 0 -1	0 -1 -1	-1 1 0	1 0 1	0 -1 1	-1 0 -1	1 1 0	0 1 -1	-1 0 1	1 -1 0
-2 -1 1	1 -1 -2	1 2 1	-2 1 -1	1 1 2	1 -2 -1	-2 -1 -1	1 2 -1	1 -1 2	-2 1 1	1 -2 1	1 1 -2
twinning systems											
IM											
	-1 1 1			1 -1 1			-1 -1 1			1 1 1	
-1 1 -2	-1 -2 1	2 1 1	1 -1 -2	1 2 1	-2 -1 1	-1 -1 -2	2 -1 1	-1 2 1	1 1 -2	-2 1 1	1 -2 1
IIM											
	1 1 -1			-1 1 1			-1 1 -1			1 1 1	
1 -2 -1	-2 1 -1	1 1 2	-1 -2 1	2 1 1	-1 1 -2	-1 -2 -1	-1 1 2	2 1 -1	1 -2 1	1 1 -2	-2 1 1
IIIM											
	1 -1 1			1 1 -1			1 -1 -1			1 1 1	
-2 -1 1	1 -1 -2	1 2 1	-2 1 -1	1 1 2	1 -2 -1	-2 -1 -1	1 2 -1	1 -1 2	-2 1 1	1 -2 1	1 1 -2

Table 3. $\langle 112 \rangle$ true twinning directions for A1 ($[\bar{1}10]$) crystals deformed in **tension**

The first rows specify all possible twinning planes and directions, the second rows indicate whether these direction point in the twinning (**tw**) or antitwining (**at**) sense or whether the loading direction is parallel to the twinning plane (**0**). The first column gives the directions of loading in three considered variants.

A1 IM $[\bar{1}10]$	c ($\bar{1}11$) $[\bar{1}1\bar{2}]$	d ($1\bar{1}1$) $[1\bar{1}\bar{2}]$	b ($\bar{1}\bar{1}1$) $[\bar{1}\bar{1}\bar{2}]$	a (111) $[11\bar{2}]$
	tw	tw	0	0
A1 IIM $[\bar{1}01]$	-b ($11\bar{1}$) $[112]$	c ($\bar{1}11$) $[\bar{1}1\bar{2}]$	-d ($\bar{1}\bar{1}1$) $[\bar{1}\bar{1}\bar{2}]$	a (111) $[11\bar{2}]$
	at	at	0	0
A1 IIIM $[0\bar{1}1]$	d ($1\bar{1}1$) $[1\bar{1}\bar{2}]$	-b ($11\bar{1}$) $[112]$	-c ($1\bar{1}\bar{1}$) $[1\bar{1}\bar{2}]$	a (111) $[11\bar{2}]$
	at	at	0	0

The twinning sense is **reversed** for the **compressive** deformation.

The observed deformation modes according to [5] are marked in Tables 1, 2 and 4, 5 in bold. The deformation systems are arranged in such a way that the systems in each column have the same Schmid factor. Both the slip and twinning systems were systematically generated for all six possible variants. The IT twin variant is equivalent to the IM matrix variant, and similarly, IIT is equivalent to IIIM and IIIT to IIM. Consequently, it is sufficient to present the results only for three matrix variants. The same deformation modes were indeed observed both for tensile and compressive deformation in the following pairs of variants: IM and IT, IIIM and IIT, IIM and IIIT [5].

Table 4. Observed deformation modes in **A2** ($[\bar{1}\bar{1}2]$) PST crystal deformed in **tension**

The slip and twinning systems are arranged in such a way that the systems in each column have the same Schmid factors marked at the top of the table. The directions of ordinary dislocations and of true twinning with the largest Schmid factors are underlined. The observed systems [5] are in bold.

Schmid factors											
-0.272	-0.136	<u>0.408</u>	0.272	<u>-0.408</u>	0.136	0.000	-0.272	0.272	0.000	0.000	0.000
-0.314	<u>0.393</u>	-0.079	-0.314	-0.079	<u>0.393</u>	-0.314	0.157	0.157	0.000	0.000	0.000
slip systems											
IM											
	<u>-1 1 1</u>			<u>1 -1 1</u>			<u>-1 -1 1</u>			<u>1 1 1</u>	
1 1 0	-1 0 -1	0 -1 1	-1 -1 0	1 0 -1	0 1 1	-1 1 0	0 -1 -1	1 0 1	1 -1 0	0 1 -1	-1 0 1
-1 1 -2	-1 -2 1	2 1 1	1 -1 -2	1 2 1	-2 -1 1	-1 -1 -2	2 -1 1	-1 2 1	1 1 -2	-2 1 1	1 -2 1
IIM											
	<u>1 1 -1</u>			<u>-1 1 1</u>			<u>-1 1 -1</u>			<u>1 1 1</u>	
1 0 1	0 -1 -1	-1 1 0	-1 0 -1	0 -1 1	1 1 0	1 0 -1	-1 -1 0	0 1 1	-1 0 1	1 -1 0	0 1 -1
1 -2 -1	-2 1 -1	1 1 2	-1 -2 1	2 1 1	<u>-1 1 -2</u>	-1 -2 -1	-1 1 2	2 1 -1	1 -2 1	1 1 -2	-2 1 1
IIIM											
	<u>1 -1 1</u>			<u>1 1 -1</u>			<u>1 -1 -1</u>			<u>1 1 1</u>	
0 1 1	-1 -1 0	1 0 -1	0 -1 -1	-1 1 0	1 0 1	0 -1 1	-1 0 -1	1 1 0	0 1 -1	-1 0 1	1 -1 0
-2 -1 1	<u>1 -1 -2</u>	1 2 1	-2 1 -1	1 1 2	1 -2 -1	-2 -1 -1	1 2 -1	1 -1 2	-2 1 1	1 -2 1	1 1 -2
twinning systems											
IM											
	<u>-1 1 1</u>			<u>1 -1 1</u>			<u>-1 -1 1</u>			<u>1 1 1</u>	
-1 1 -2	-1 -2 1	2 1 1	1 -1 -2	1 2 1	-2 -1 1	-1 -1 -2	2 -1 1	-1 2 1	1 1 -2	-2 1 1	1 -2 1
IIM											
	<u>1 1 -1</u>			<u>-1 1 1</u>			<u>-1 1 -1</u>			<u>1 1 1</u>	
1 -2 -1	-2 1 -1	1 1 2	-1 -2 1	2 1 1	<u>-1 1 -2</u>	-1 -2 -1	-1 1 2	2 1 -1	1 -2 1	1 1 -2	-2 1 1
IIIM											
	<u>1 -1 1</u>			<u>1 1 -1</u>			<u>1 -1 -1</u>			<u>1 1 1</u>	
-2 -1 1	<u>1 -1 -2</u>	1 2 1	-2 1 -1	1 1 2	1 -2 -1	-2 -1 -1	1 2 -1	1 -1 2	-2 1 1	1 -2 1	1 1 -2

Table 5. Observed deformation modes in **A2** ($[\bar{1}\bar{1}\bar{2}]$) PST crystal deformed in **compression**

Schmid factors											
.272	.136	<u>-.408</u>	-.272	<u>.408</u>	-.136	.000	.272	-.272	.000	.000	.000
.314	<u>-.393</u>	.079	.314	.079	<u>-.393</u>	.314	-.157	-.157	.000	.000	.000
slip systems											
IM											
1 1 0	<u>-1 0 -1</u>	0 -1 1	-1 -1 0	1 0 -1	0 1 1	-1 1 0	<u>0 -1 -1</u>	1 0 1	1 -1 0	0 1 -1	-1 0 1
<u>-1 1 -2</u>	-1 -2 1	2 1 1	<u>1 -1 -2</u>	1 2 1	-2 -1 1	<u>-1 -1 -2</u>	2 -1 1	-1 2 1	1 1 -2	-2 1 1	1 -2 1
IIM											
<u>1 0 1</u>	0 -1 -1	<u>-1 1 0</u>	-1 0 -1	0 -1 1	1 1 0	1 0 -1	-1 -1 0	0 1 1	-1 0 1	1 -1 0	0 1 -1
1 -2 -1	-2 1 -1	<u>1 1 2</u>	-1 -2 1	2 1 1	<u>-1 1 -2</u>	-1 -2 -1	-1 1 2	2 1 -1	1 -2 1	1 1 -2	-2 1 1
IIIM											
0 1 1	-1 -1 0	1 0 -1	<u>0 -1 -1</u>	<u>-1 1 0</u>	1 0 1	0 -1 1	-1 0 -1	1 1 0	0 1 -1	-1 0 1	1 -1 0
-2 -1 1	<u>1 -1 -2</u>	1 2 1	-2 1 -1	<u>1 1 2</u>	1 -2 -1	-2 -1 -1	1 2 -1	1 -1 2	-2 1 1	1 -2 1	1 1 -2
twinning systems											
IM											
-1 1 -2	-1 -2 1	2 1 1	1 -1 -2	1 2 1	-2 -1 1	-1 -1 -2	2 -1 1	-1 2 1	1 1 -2	-2 1 1	1 -2 1
IIM											
1 -2 -1	-2 1 -1	1 1 2	-1 -2 1	2 1 1	<u>-1 1 -2</u>	-1 -2 -1	<u>-1 1 2</u>	2 1 -1	1 -2 1	1 1 -2	-2 1 1
IIIM											
-2 -1 1	<u>1 -1 -2</u>	1 2 1	-2 1 -1	1 1 2	1 -2 -1	-2 -1 -1	1 2 -1	<u>1 -1 2</u>	-2 1 1	1 -2 1	1 1 -2

Table 6. $\langle 112 \rangle$ true twinning directions for **A2** ($[\bar{1}\bar{1}\bar{2}]$) crystals deformed in **tension**

The first rows specify all possible twinning planes and directions, the second rows indicate whether these direction point in the twinning (**tw**) or antitwinning (**at**) sense or whether the loading direction is parallel to the twinning plane (**0**). The first column gives the directions of loading in three considered variants.

A2 IM $[\bar{1}\bar{1}\bar{2}]$	c $(\bar{1}11)$ $[\bar{1}\bar{1}\bar{2}]$	d $(1\bar{1}\bar{1})$ $[\bar{1}\bar{1}\bar{2}]$	b $(\bar{1}\bar{1}\bar{1})$ $[\bar{1}\bar{1}\bar{2}]$	a (111) $[\bar{1}\bar{1}\bar{2}]$
	at	at	at	0
A2 IIM $[1\bar{2}1]$	-b $(11\bar{1})$ $[112]$	c $(\bar{1}\bar{1}\bar{1})$ $[\bar{1}\bar{1}\bar{2}]$	-d $(\bar{1}\bar{1}\bar{1})$ $[\bar{1}\bar{1}\bar{2}]$	a (111) $[11\bar{2}]$
	at	tw	tw	0
A2 IIIM $[2\bar{1}1]$	d $(1\bar{1}\bar{1})$ $[\bar{1}\bar{1}\bar{2}]$	-b $(11\bar{1})$ $[112]$	-c $(\bar{1}\bar{1}\bar{1})$ $[11\bar{2}]$	a (111) $[11\bar{2}]$
	tw	at	tw	0

The twinning sense is **reversed** for the **compressive** deformation.

Because of a high symmetry of the $\langle 101 \rangle$ loading axis, the Schmid factors attain the maximum magnitudes of 0.408 for four slip systems of the $\langle 101 \rangle$ type and they are zero for the other systems (see Tables 1 and 2). For the $\langle 121 \rangle$ loading axis, there are only two slip systems with the largest Schmid factor while four systems experience the Schmid factor reaching two thirds of the largest one and two systems only one third (see Tables 4 and 5). Under the largest Schmid factor, the ordinary dislocations are always observed to contribute to the plastic flow, however, only at most one half of the $\langle 101 \rangle$ superdislocations are active. The slip directions of ordinary dislocations with the largest Schmid factor are underlined in Tables 1, 2 and 4, 5. When the $\langle 101 \rangle$ superdislocation is observed for the tensile loading it is passive for compression and *vice versa*. It clearly indicates that their motion have asymmetrical nature. Each $\langle 121 \rangle$ direction in Tables 1, 2 and 4, 5 is perpendicular to the $\langle 101 \rangle$ superlattice direction above it. Hence the $1/2\langle 101 \rangle$ superpartial can be dissociated into Shockley partials with the remaining two $\langle 121 \rangle$ directions from which only one is of the $\langle 112 \rangle$ SISF type. Let us consider the sign of projection of the $\langle 101 \rangle$ superlattice Burgers vector to this $\langle 112 \rangle$ direction taking into account the sign of the Schmid factor for the respective $\langle 101 \rangle$ superdislocation. When this sign is negative for the slip systems with the largest Schmid factor, the $\langle 101 \rangle$ superdislocation slip is observed with the exception of two cases. Hence we can conclude that from three slip systems in the three matrix variants with the largest Schmid factors that one corresponding to the ordinary dislocations is always active. But from the remaining two superdislocation slips, only one can be active according to the sense of acting stress determined as described above.

For the $\langle 101 \rangle$ loading direction, the Schmid factor in the $\langle 121 \rangle$ direction attains the largest magnitude of 0.471, one half of it or zero. On the other hand for the $\langle 121 \rangle$ loading, the Schmid factor possesses the largest magnitude of 0.393 which is five times greater than the smallest non-zero value of 0.079 and the second largest magnitude is four times greater than 0.079. The twinning systems with the largest Schmid factors are underlined in Tables 1, 2 and 4, 5. Corresponding deformation twins propagate in the twinning direction only for deformation in tension. These directions take the antitwinning sense when the tensile loading is reversed into compressive. Deformation twinning is then observed for some of the systems with the second largest Schmid factor but not for all of them.

Let us discuss now in more detail the observed deformation modes for four different types of experiments described in Tables 1, 2 and 4, 5. The ordinary dislocations are easily mobile and their underlined slip directions with the largest Schmid factor are always active.

A1 crystals strained in *tension* (Table 1)

Twinning occurs only in one variant (IM) on two systems with the largest Schmid factors. Their twinning directions are underlined. Four slip directions of superdislocations are not permitted in IM (grey-highlighted). When both twinning systems are equally active, the resulting strain is parallel to the (111) lamellar interfaces.

An appropriate combination of $1/2\langle 112 \rangle$ and $1/2\langle 110 \rangle$ slips can lead to the strain in the $\langle 101 \rangle$ direction. Two cases can be distinguished: If the $\langle 101 \rangle$ direction is parallel to the lamellar interfaces, both the $\langle 101 \rangle$ superdislocations and the combination of the $1/2\langle 112 \rangle$ and $1/2\langle 110 \rangle$ slips give the strains parallel to (111). If the $\langle 101 \rangle$ direction is not parallel to (111), only a strain of equal amount due to the $\langle 101 \rangle$ superdislocations on the one side, and the $1/2\langle 112 \rangle$ and $1/2\langle 110 \rangle$ dislocations on the other side can provide a resulting strain parallel to (111).

A1 crystals strained in compression (Table 2)

Twinning on the systems with the largest Schmid factor is not permitted (grey-highlighted), and thus the systems with the second largest may carry plastic deformation. Two such systems out of four possible are indeed observed, twinning in the $[112]$ direction is not active. When the associated ordinary slip is not parallel to the interfaces, it can be combined with the twinning to give a total strain in a particular variant parallel to (111) . However, when the ordinary slip is already parallel to (111) , it cannot turn the twinning strain into the (111) plane. Only if the amount of twinning is zero in a combination with the associated ordinary slip (parallel to (111)), the resulting strain can be parallel to (111) . This may be the reason why two twinning systems with the second largest Schmid factor are not active and the other two active are. Those that are not active are twinings in the $[112]$ direction that is associated with the $1/2[\bar{1}10]$ ordinary dislocations.

Similarly, when two superdislocation slips are permitted in IM but one of their slip directions is parallel to (111) , it can not be combined with the other one to give a strain parallel to (111) . Hence only one out of two superdislocation slips on each glide plane is observed, that one which is parallel to (111) .

The $1/2\langle 112 \rangle$ slip that is not parallel to (111) needs the associated ordinary slip to make the strain parallel to (111) . However, the ordinary slip with zero Schmid factor is of no help, and thus the permitted $1/2\langle 112 \rangle$ slips with the largest Schmid factor in IM are not active.

A2 crystals strained in tension (Table 4)

Twinning occurs in different variants for two systems with the largest Schmid factors. Their twinning directions are again underlined. In both cases the twinning is accompanied by the ordinary slip in spite of the fact that the respective Schmid factor is very low (0.136 only). The ordinary slip with the largest Schmid factor (underlined) is parallel to (111) . Only an appropriate combination of twinning with the associated ordinary slip can lead to the strain parallel to the (111) interfaces separately in each variant (IIM or IIIM).

The superdislocation slip with the largest Schmid factor is parallel to (111) on two different slip planes in IM. Moreover, the $1/2\langle 112 \rangle$ slip with the second largest Schmid factor is also activated when it is associated with the ordinary slip. However, when the Schmid factor for the ordinary slip is zero, the $1/2\langle 112 \rangle$ slip is not active. Similarly, not all the ordinary slips with the second largest Schmid factor are observed. Only those which are associated with the $1/2\langle 112 \rangle$ slip. Naturally, when both Schmid factors for the $1/2\langle 112 \rangle$ and $1/2\langle 110 \rangle$ slips are low, both slip systems are passive.

A2 crystals strained in compression (Table 5)

Out of three twinning systems with the second largest Schmid factor, two are active. In these two cases, the twinning is combined with the ordinary slip with the second largest Schmid factor. The ordinary slip associated with the third twinning system has zero Schmid factor. This is apparently the reason why it is not active.

The observed $1/2\langle 112 \rangle$ slip with the largest Schmid factor is accompanied by the ordinary slip with very small Schmid factor (0.136 only).

Only two out of four ordinary slips with the second largest Schmid factor are active, those that are combined either with the twinning or $1/2\langle 112 \rangle$ slip of sufficiently high Schmid factor. For the other two ordinary slips, the associated Schmid factor for the $1/2\langle 112 \rangle$ slip is too low.

Let us summarize the basic points discussed above. The $\langle 101 \rangle$ slip systems with the largest Schmid factors are always activated in the case of the $1/2\langle 110 \rangle$ ordinary dislocations. However, for the $\langle 101 \rangle$ superdislocations, they are active only if the acting force has the right sense. Twinning can obviously occur only in the twinning direction, and it happens not only

on the twinning systems with the largest Schmid factor for tension but also for the second significantly lower Schmid factor in compression. When the applied stress acts in the antitwinning direction, the $1/2\langle 112 \rangle$ slip can be activated provided that the force acting on the conjugate ordinary dislocations is not zero.

EFFECT OF LAMELLAR INTERFACES

The activity of various deformation modes can be explained taking into account

- a) the magnitude of acting forces due to the applied stress (Schmid factors),
- b) the asymmetry of deformation processes (twinning and superdislocation glide), and
- c) the effect of lamellar interfaces.

It has been shown above that some deformation modes are active while the others under the same applied stress that could propagate the strain in the permitted direction are not active. This fact can be explained assuming that the total strain in each variant should be parallel to the (111) interface plane as discussed already in the foregoing section. The allowed plastic deformation modes along the directions inclined to the lamellae are activated only in combination with another deformation mode leading to the resulting shear parallel to the lamellae. This channelling of plastic deformation parallel to the planes with zero Schmid factor is a remarkable phenomenon that has a broader importance for lamellar structures in general.

The interfaces are obviously efficient obstacles for dislocation motion. Dislocation processes taking place at the interfaces have been recently studied by *in situ* [10,11] and *post mortem* [12,13] electron microscopy. It was found, for example, that the strain of an incoming twin formed by the $1/6\langle 112 \rangle$ Shockley partials can be transferred to the neighbouring lamella across the 120° interface by the ordinary and super-dislocations according to the reaction

$$6 \ 1/6\langle 112 \rangle^I = 2 \ 1/2\langle 110 \rangle^{II} + \langle 101 \rangle^{II} .$$

Since the Burgers vectors belong to two different crystals separated by the interface, the expression above indicates only the number and types of dislocations but not the particular crystallographic directions. The dislocations propagate along the $\{111\}$ plane in continuation of the initial glide plane. Another reaction can be written for the transition across the twin (180°) interface

$$3 \ 1/6\langle 112 \rangle^I = 3 \ 1/6\langle 112 \rangle^{II} + 1/2\langle 110 \rangle^{II} + 1/2\langle 110 \rangle^I .$$

In this case the dislocations lie on the mirror symmetric glide planes. It is seen that the motion of Shockley partials of twinning is accompanied in both lamellae by the glide of ordinary dislocations. Because of the difficulties to observe *in situ* what is happening at the interfaces, the role of interface dislocations was analyzed *post mortem* and the following reaction was proposed

$$3 \ 1/6\langle 112 \rangle^I = 3 \ 1/6\langle 112 \rangle^{II} + 2 \ 1/2\langle 110 \rangle^{II} + 2 \ 1/6\langle 112 \rangle^{I-II} .$$

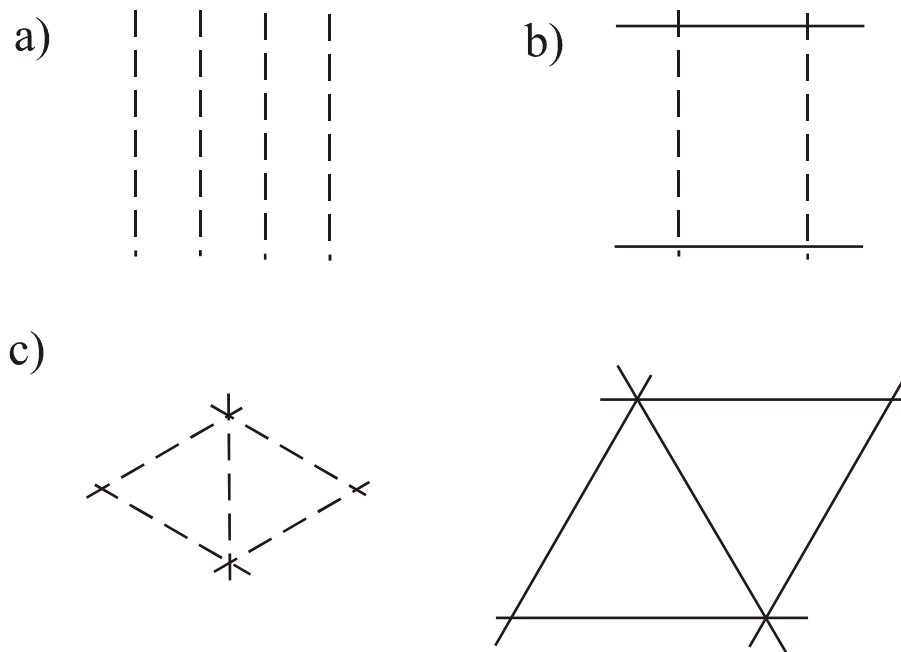


Fig. 2. Different arrays of interfacial dislocations compensating the misfit of shear type. Dashed lines represent $1/6\langle 112 \rangle$ dislocations, full lines $1/2\langle 110 \rangle$ dislocations.

The incoming and outgoing planes are mirror symmetric with respect to the twin interface. Notice that the last term represents interfacial dislocations with the Burgers vector parallel to the interface. Propagation of outgoing Shockley partials is again associated with the ordinary dislocations. It can be concluded that the twinning is linked with the motion of ordinary dislocations arising from the reactions at the interfaces during the transfer of plastic deformation.

It has been demonstrated in [14,15] that the misfit caused by the tetragonality of the $L1_0$ structure on the 120° and 60° (pseudotwin) interfaces can be compensated by the networks of interfacial dislocations of various types. In principle, just one set of screw dislocations (Fig. 2a) would be sufficient, but the same misfit of shear type can be compensated also by two (Fig. 2b) or three (Fig. 2c) dislocation arrays. The Burgers vectors of interfacial dislocations lie at the interface. An array of dislocations with the Burgers vector perpendicular to the interface would give rise to a tilt deviation from this interface of special character and such deviation is likely to increase the interfacial energy.

The interfacial dislocations are apparently mobile along the interface, and can thus increase the flexibility of plastic deformation. The macroscopic measurements [5,16] show that the strain in the lamellae is parallel to the interfaces in the PST crystals loaded along the lamellae, i.e. the resulting strain is parallel to the plane with zero resolved shear stress. This is a consequence of the fact that the deformation modes inclined to the lamellae are combined in such a way to give strain not interfering with the interfaces.

GRAIN BOUNDARIES BETWEEN PST CRYSTALS

As it is described in detail in [5,17,18], the mechanical properties of PST crystals are strongly anisotropic and depend on the orientation of the loading axis with respect to the normal to the lamellar interfaces. With the exception of the loading axis normal to the lamellae, the plastic deformation takes place parallel to the lamellar interfaces. This behaviour is natural for the inclination of the loading axis close to 45° as the slip plane parallel to the interfaces experiences the largest Schmid factor. However, it is rather unexpected for the loading axis parallel to the interfaces when the Schmid factor on the (111) plane parallel to the interfaces is zero and the plastic deformation takes place on the $\{111\}$ planes inclined to the lamellae.

Since both elastic as well as plastic deformation of PST crystals, i.e. of the lamellar colonies, have anisotropic nature, it is important what is happening at the grain boundaries that separate the neighbouring crystals in polycrystals. The effect of the grain boundaries can be treated on different levels: The additional stresses arise in the vicinity of the boundary due to compatibility requirements on the macroscopic level of elastic continuum. The boundary structure including the steps and ledges, and dislocation reactions leading to the formation of residual boundary dislocations can be taken on a mesoscopic level. Finally, the deformation processes can be affected on the atomic level by the boundary structure and chemistry, segregation phenomena etc. In this section, only a model for evaluation of stress redistribution will be briefly introduced as a tool for theoretical predictions of possible deformation modes that can be active in the bicrystal in addition to those caring plastic deformation in single-crystals.

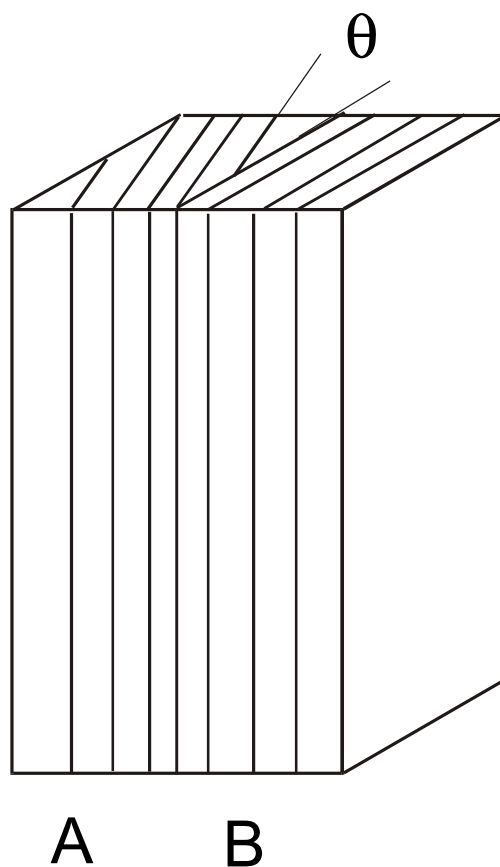


Fig. 3. Two grains A and B, representing two lamellar colonies, constitute a bicrystal.

Imagine a bicrystal composed of two joint PST crystals as depicted in Fig. 3. Contrary to the lamellar interfaces, the grain boundaries between PST crystals need not be of special character since their misorientation can be in principle arbitrary. Nevertheless, we will consider only the bicrystals with the normal to the grain boundary perpendicular to a chosen growth axis (e.g. $[\bar{1}10]$ for A1 or $[\bar{1}\bar{1}2]$ for A2 crystals). There are still two angles characterizing the geometry of the bicrystal, namely, the misorientation angle between two PST crystals and the inclination of the boundary plane with respect to the lamellar interfaces. We can reduce them to just one parameter if we consider only the lamellae in the grain B parallel to the grain boundary as illustrated in Fig. 3. When the angle θ is zero we get just a continuous PST single crystal without any interface at the grain boundary. For $\theta = 180^\circ$, the grain boundary becomes a true twin interface, and hence there is again no grain boundary in the sense defined above. For the chosen normal to the grain boundary in the grain B, the angle θ determines both the grain misorientation and inclination of the boundary plane.

As discussed above the PST crystal is composed of different variants of the $L1_0$ -phase with the tetragonal symmetry. However, the overall average symmetry of a system which components are rotated by the multiples of 60° above a fixed rotation axis (perpendicular to the lamellar interfaces) is hexagonal with the c-axis parallel to the interface normal. Obviously, the occurrence of the α_2 phase, that has the hexagonal symmetry itself, does not alter this symmetry. Therefore, the hexagonal symmetry can be considered in the calculations of compatibility stresses for homogeneous elastic and plastic straining of PST grains. Nevertheless, since the properties of the $\langle 101 \rangle$ dislocations depend on the orientation of the tetragonal axis in each variant, the tetragonality has to be respected on the mesoscopic level of the forces acting on dislocations.

Let us denote the imposed elastic and plastic strains in the separate crystals A and B as e_{ij}^{Ae} , e_{ij}^{Be} and e_{ij}^{Ap} , e_{ij}^{Bp} , respectively. Providing that the difference between the strains in the joint grains is not too large such a difference can be accommodated by the additional compatibility strains (e_{ij}^A and e_{ij}^B) of elastic nature. The conditions of strain compatibility in the coordinate system of the bicrystal, where the axis x_2 is perpendicular to the grain boundary, that can be expressed as

$$\varepsilon_{ij}^A = \varepsilon_{ij}^B \quad \text{for } ij = 11, 33, 13, \quad (1)$$

must be fulfilled by the total strains

$$\varepsilon_{ij}^K = e_{ij}^{Ke} + e_{ij}^{Kp} + e_{ij}^K \quad \text{for } K = A, B.$$

The difference between the strains in the separate crystals

$$\Delta e_{ij} = e_{ij}^{Be} + e_{ij}^{Bp} - e_{ij}^{Ae} - e_{ij}^{Ap}$$

will then give rise to the additional stress tensor τ_{ij} . The compatibility stresses can be calculated using the equation

$$\begin{pmatrix} \tau_{11} \\ \tau_{33} \\ \tau_{13} \end{pmatrix} = -\text{sgn } x_2 \begin{pmatrix} s_{11}^+ & s_{13}^+ & s_{15}^+ \\ s_{13}^+ & s_{33}^+ & s_{35}^+ \\ s_{15}^+ & s_{35}^+ & s_{55}^+ \end{pmatrix}^{-1} \begin{pmatrix} \Delta e_{11} \\ \Delta e_{33} \\ \Delta e_{13} \end{pmatrix} \quad (2)$$

where s_{ij}^+ are sums of elastic compliances in the usual two-index notation in our case possessing hexagonal symmetry

$$s_{ij}^+ = s_{ij}^A + s_{ij}^B.$$

The first term in Eq. (2) for the additional stress τ_{ij} is the function $\text{sgn } x_2$ which is negative in the crystal A and positive in the crystal B. For more details of the calculations of compatibility stresses see [19]. The results of the application of the above described model to the A2 bicrystals can be found in [20]. It was shown that the predictions of our model agree with the observations of deformation activity in the A2(90°/0°) bicrystal deformed in tension and can be thus used to assess deformation behaviour in the bicrystals that have not been experimentally investigated.

CONCLUSIONS

Behaviour of the carriers of plastic deformation in Ti-Al intermetallics is discussed. The activity of various deformation modes is controlled by the applied stress, by the asymmetry of twinning and of superdislocation motion and by the effects of the lamellar interfaces and the grain boundaries between the lamellar colonies. According to the presented consistent picture, the twinning, as expected, can occur only in the twinning sense, but the motion of the $\langle 101 \rangle$ and $1/2\langle 112 \rangle$ superdislocations take place only in the direction determined by the antitwining sense. It can be anticipated that under the forces acting in the opposite sense, the dislocation cores are transformed into immobile locked configurations. Some phenomena caused by the interfaces such as interfacial dislocations and compatibility stresses are also briefly discussed.

Acknowledgements

This research was supported by the Grant Agency of the Academy of Sciences (A1010817/1998) and by the Ministry of Education of the Czech Republic (ME190).

REFERENCES

- [1] Yamaguchi M., Nishitani S.R. and Shirai Y.: In: *High Temperature Aluminides and Intermetallics*, S.H. Whang, C.T. Liu, D.P. Pope and J.O. Stiegler (Eds.), TMS, 1990, p. 63.
- [2] Yamaguchi M. and Inui H.: In: *Ordered Intermetallics - Physical Metallurgy and Mechanical Behaviour*, C.T. Liu, R.W. Cahn and G. Sauthoff (Eds.), Kluwer, Dordrecht, 1992, p. 217.
- [3] Zghal S., Naka S. and Couret A.: *Acta Mater.* **45**, (1997) 3005.

- [4] Inui H., Nakamura A., Oh M.H. and Yamaguchi M.: *Phil. Mag. A* **66**, (1992) 557.
- [5] Kishida K., Inui H. and Yamaguchi M.: *Phil. Mag. A* **78**, (1998) 1.
- [6] Imamura D., Hoshikawa H., Kishida K., Inui H. and Yamaguchi M.: In: *High-Temperature Ordered Intermetallic Alloys VIII*, E.P. George, M.J. Mills and M. Yamaguchi (Eds.), Mater. Res. Soc. Symp. Proc. Vol. 552, MRS, Warrendale, PA, 1999, p. KK3.9.1.
- [7] Paidar V. and Vitek V.: In: *Intermetallic Compounds, Advances*, J.H. Westbrook and R.L. Fleischer (Eds.), Vol. 3, John Wiley, Chichester, 2001, in press.
- [8] Ehmman J. and Fahnle M.: *Phil. Mag. A* **77**, (1998) 701.
- [9] Paidar V., Inui H., Kishida K. and Yamaguchi M.: *Mater. Sci. Eng. A* **233**, (1997) 111.
- [10] Zghal S., Coujou A. and Couret A.: *Phil. Mag. A* **81**, (2001) 345.
- [11] Zghal S. and Couret A.: *Phil. Mag. A* **81**, (2001) 365.
- [12] Gibson M.A. and Forwood C.T.: *Phil. Mag. A* **80**, (2000) 2747.
- [13] Forwood C.T. and Gibson M.A.: *Phil. Mag. A* **80**, (2000) 2785.
- [14] Paidar V., Zghal S. and Couret A.: *Mater. Sci. Forum* **294-296**, (1999) 385.
- [15] Paidar V., Zghal S. and Couret A.: In: *High-Temperature Ordered Intermetallic Alloys VIII*, E.P. George, M.J. Mills and M. Yamaguchi (Eds.), Mater. Res. Soc. Symp. Proc. Vol. 552, Warrendale, PA, 1999, p. KK3.2.1.
- [16] Kim M.-C., Nomura M., Vitek V. and Pope D.P.: In: *High-Temperature Ordered Intermetallic Alloys VIII*, E.P. George, M.J. Mills and M. Yamaguchi (Eds.), Mater. Res. Soc. Proc. Vol. 552, Warrendale, PA, 1999, p. KK3.1.1.
- [17] Fujiwara T., Nakamura A., Hosomi M., Nishitani S.R., Shirai Y. and Yamaguchi M.: *Phil. Mag. A* **61**, (1990) 591.
- [18] Inui H., Kishida K., Misaki M., Kobayashi M., Shirai Y. and Yamaguchi M.: *Phil. Mag. A* **72**, (1995) 1609.
- [19] Gemperlová J., Paidar V. and Kroupa F.: *Czech. J. Phys. B* **39**, (1989) 427.
- [20] Paidar V., Imamura D., Inui H. and Yamaguchi M.: *Acta Mater.* **49**, (2001) 1009.